Clim Dyn (2011) 37:1661–1669
DOI 10.1007/s00382-010-0938-4

Predictable climate dynamics of abnormal East Asian winter monsoon: once-in-a-century snowstorms in 2007/2008 winter

Zhiwei Wu · Jianping Li · Zhihong Jiang · Jinhai He

Received: 9 March 2010 / Accepted: 22 October 2010 / Published online: 5 November 2010
© Springer-Verlag 2010

Abstract In 2008 (January–February), East Asia (EA) experiences the most severe and long-persisting snowstorm in the past 100 years. Results in this study show that 2007/2008 winter is dominant by the third principal mode of the East Asian winter monsoon (EAWM) which explains 8.7% of the total surface air temperature variance over EA. Significantly distinguished from the first two leading modes, the third mode positive phase features an increased surface pressure over the northwestern EA, an enhanced central Siberian high (CSH), a strengthened and northwestward extended western Pacific subtropical high (WPSH) and anomalously strong moisture transport from western Pacific, Arabian Sea and Bay of Bengal to EA. It also exhibits an intimate linkage with the sea surface temperature anomalies (SSTAs) in the Arctic Ocean areas adjacent to northern Eurasian continent, central North Pacific and northeastern Pacific. Such SSTAs emerge in prior autumn and persist through ensuing winter, signifying precursory conditions for the anomalous third EAWM mode. Numerical experiments with a simple general circulation model demonstrate that the Arctic SSTAs excite geo-potential height anomalies over northern Eurasian continent and impacts on the CSH, while the extra-tropical Pacific SSTAs deform the WPSH. Co-effects of them play crucial roles on origins of the third EAWM mode. Based on these results, an empirical model is established to predict the third mode of the EAWM. Hindcast is performed for the 1957–2008 period, which shows a quite realistic prediction skill in general and good prediction ability in the extreme phase of the third mode of the EAWM such as 2007/2008 winter. Since all these predictors can be readily monitored in real time, this empirical model provides a real time forecast tool and may facilitate the seasonal prediction of high-impact weather associated with the abnormal EAWM.

Keywords Seasonal prediction · East Asian winter monsoon · Snowstorm

Z. Wu · J. Li (✉)
LASG, Institute of Atmospheric Physics,
Chinese Academy of Sciences, 100029 Beijing, China
e-mail: ljp@lasg.iap.ac.cn

Z. Wu
Meteorological Research Division, Environment Canada,
Dorval, QC H9P 1J3, Canada

Z. Jiang · J. He
Key Laboratory of Meteorological Disaster of Ministry
of Education, Nanjing University of Information Science
and Technology, Nanjing, China

1 Introduction

In 2008 (January–February), East Asia (EA) (particularly China) experiences a record-breaking (most severe in many decades) and long-persisting snowstorm and leads to huge property loss and hundreds of people's death. In the meanwhile, severe snowstorms also attacked North America and Russia. The central Asia even experienced the first snowfall in the last 100 years (http://www.chinajilin.com.cn/content/2008-02/03/content_1141936.htm). Such series of disastrous climate events inevitably receive broad scientific foci and trigger fervent research interests on the East Asian winter monsoon (EAWM) (e.g., Tao and Wei 2008; Ding et al. 2008; Wen et al. 2009; Hong and Li 2009; Bao et al. 2010). Inspecting possible physical mechanisms responsible for the abnormal EAWM in 2007/2008 winter, especially its predictability sources, could not only improve understanding the variation rules of the EAWM, but also

benefit seasonal prediction of high-impact weather associated with the abnormal EAWM.

The EAWM exhibits pronounced oscillations from interannual to multi-decadal timescales (e.g., Li 1955; Tao 1957; Ding and Krishnamurti 1987; Chan and Li 2004; Jhun and Lee 2004; Chang et al. 2006, 2009; Li and Bates 2007; Wu et al. 2009a). Wang et al. (2010) found that the EAWM is usually dominated by two distinct principal modes, namely, the northern mode and the southern mode in terms of the surface air temperature (SAT) variability. These two leading modes bear distinguished circulation structures and different causes. El Niño-Southern Oscillation (ENSO), snow cover over the southern and northeastern Siberian, and sea surface temperature (SST) of North Atlantic and tropical Indian Ocean are major impact factors for the two leading modes. In 2007/2008 winter, the EAWM displayed many distinct features which neither belong to a typical first mode EAWM nor a second mode documented by Wang et al. (2010). Since most previous studies chose to consider it as a once-in-a-century (or extremely rare) case, they focused more on its uniqueness than its universality and investigations were conducted along this line. For example, Tao and Wei (2008) emphasized roles of the sustaining blocking high in the mid-high latitudes over EA based on synoptic scale analysis of the snowstorm events in January 2008. Ding et al. (2008) suggested the strong La Niña event in 2007/2008 winter provides a climate background for invasion of cold air into South China and the persistence of circulation anomalies over the Eurasian continent is the direct cause of the snowstorms. Wen et al. (2009) believed these snowstorms were closely linked to the change in the Middle East jet stream and the anomalous western Pacific subtropical high (WPSH). Besides the above mentioned, the tropical intraseasonal oscillation and anomalous Tibetan Plateau warming are also suggested to be responsible for the anomalous 2007/2008 snowstorms (Hong and Li 2009; Bao et al. 2010).

Although the catastrophic consequences of the 2007/2008 winter snowstorms are unprecedented or once-in-a-century (Zheng 2008; Wang et al. 2008), several similar cases do occur in the past 50 years. This provides the feasibility of investigating the general features of the 2007/2008-like EAWM anomalies and their predictability sources. This study attempts to answer the following questions: What kind of principal mode dominates the abnormal 2007/2008 winter monsoon over EA? What are the common features of the 2007/2008-like EAWM anomalies? The most important issue might be how to predict such winter monsoon anomalies.

This paper is structured as follows. Section 2 describes the datasets, the numerical model and the methodology used in this study. Section 3 suggests that 2007/2008 winter is dominated by the third principal mode of the EAWM. Section 4 investigates the predictability sources of the third mode and Sect. 5 discusses the possible physical mechanisms on the 2007/2008-like EAWM anomalies with a simplified general circulation model (SGCM). In Sect. 6, an empirical model is established to forecast the EAWM third mode based on the above predictability sources. Hindcast is performed for the 1957–2008 period. The last section summarizes major findings and discusses some outstanding issues.

2 Data, model and methodology

The main datasets employed in this study include (1) monthly observed SAT and precipitation data from 160 gauge stations across China for the 1957–2009 period; (2) European Centre for Medium-Range Weather Forecasts (ECMWF) 40-year reanalysis data (ERA-40; Uppala et al. 2005) and ERA-interim reanalysis datasets; (3) the Met Office Hadley Centre's sea ice and SST datasets gridded at $1.0° \times 1.0°$ resolution (Rayner et al. 2003). To maintain temporal homogeneity, the 2002–2009 ERA-interim data were adjusted by removing the climatological difference between the ERA-40 and ERA-interim datasets. In this study, winter (December, January, and February or DJF) mean anomalies are defined by the deviation of DJF mean from the long-term (1958–2008) mean climatology.

All the numerical experiments presented in this paper are based on the SGCM first developed by Hoskins and Simmons (1975). The resolution used here is triangular 31, with ten equally spaced sigma levels (Lin and Derome 1996). An important feature of this model is that it uses a time-averaged forcing calculated empirically from observed daily data. As shown in Hall (2000), this model is able to reproduce remarkably realistic stationary planetary waves and the broad climatological characteristics of the transients are in general agreement with observations.

To reveal the leading modes of the EAWM, we performed EOF analysis of the SAT over EA (10°–60°N, 100°–140°E). The EOF analysis was carried out by constructing a correlation matrix to eliminate the geographical influences. As such, the eigenvectors (spatial patterns) are non-dimensional.

3 Distinct third principal mode of the EAWM variability

Figure 1 presents the spatial patterns and the corresponding principal components (PCs) of the three leading modes of the EAWM SAT variability. The two leading modes bear similar spatial patterns with the northern and southern

modes documented in Wang et al. (2010) (Fig. 1a, c). It is of interest to notice that the PC3 in 2007/2008 winter reaches the highest value within the past five decades (Fig. 1f). The third mode accounts for around 8.7% of the total SAT variances, while the fourth mode explains 5.4% of the total SAT variances. The eigenvalues of the leading modes suggest that EOF3 is significantly distinguished from EOF1 and EOF2 and other modes in terms of sampling error above the 95% confidence level (North et al. 1982). The spatial pattern of EOF3 shows that during a positive phase of the third mode, anomalous cold SAT tends to occur in southern China-west Mongolia and anomalous warm in central Siberia and Philippine Sea, and vice versa.

Since the third mode explains around 8.7% of the total SAT variance, it will not become dominant in a year unless the other leading modes carry relatively small variance for this year. In 2007/2008 winter, the third mode can explain more than 70% of the total SAT variance, which is the highest in the past 52 years (Fig. 2a). As a matter of fact, totally there were four winters in which the third mode becomes dominant and accounts for more than 40% of the total variance for the 1957–2008 period. Using observational data at 160 gauge stations across China, as expected, 2007/2008 does exhibit a typical high PC3 winter feature in terms of the SAT spatial pattern, namely, anomalous cold SAT in southern China and anomalous warm in northeastern China (color shadings in Fig. 2a). The spatial patterns of the observed SAT in the other three PC3 winters (color shadings in Fig. 2b–d) are similar to that in 2007/2008 winter (color shadings in Fig. 2a). In addition, the observed precipitation anomalies of the first three winters share a similar pattern, in spite that those in 1971/1972 exhibit some differences (contours in Fig. 2).

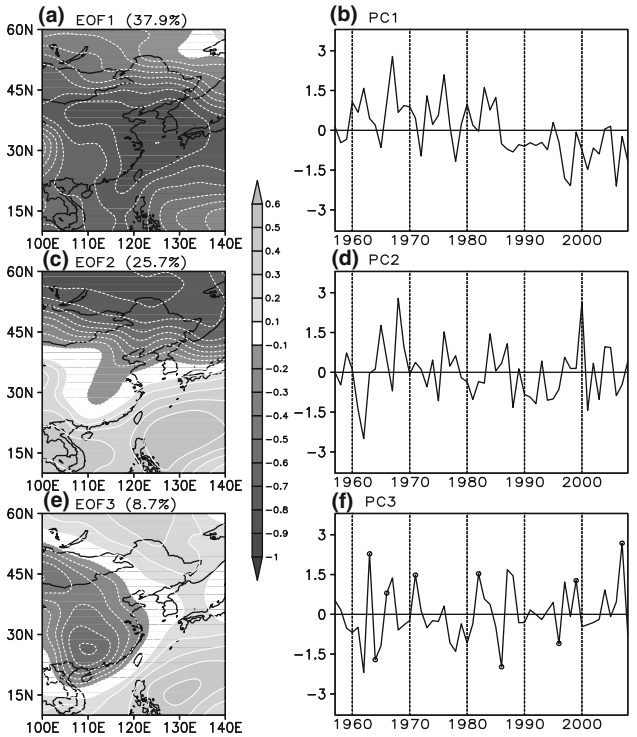

Fig. 1 *Upper panels* **a** spatial pattern and **b** the corresponding time coefficient of the first EOF mode of the winter (DJF) mean 2 m surface air temperature (SAT) in the east Asian winter monsoon (EAWM) domain (10°–60°N, 100°–140°E). *Middle panels* **c** and **d**, and *lower panels* **e** and **f** same as in **a** and **b** but for the second and the third mode. The *numbers* in the *brackets* indicate fractional variance of the EOF modes. All values are non-dimensional as they are derived from correlation coefficient matrix. The blank circles denote the high and low PC3 winters as defined in the paper

Figure 3 shows the composite difference of circulation anomalies between the high and low PC3 winters (high minus low). Note that the high or low PC3 winters in this study refer to those in which the third mode is dominant and accounts for more than 25% of the total variance. There are six high PC3 and three low PC3 winters in total from 1957 through 2008 (see those blank circles in Fig. 1f). At lower troposphere, a notable positive sea-level pressure (SLP) center occupies northern EA with a SLP ridge extending northwestward and significant anticyclonic winds. This pattern reflects a route of cold air intrusion via a "northwest pathway". Negative SLP anomalies control Tibetan Plateau, which favors moisture transport from the Bay of Bengal toward southern China along the southern flank of the Plateau. A pronounced inverse trough and cyclonic winds prevail over Philippine and South China Sea, which indicates a warm and moist air transport from Philippine Sea and western Pacific. There are large pressure gradient between northern China and Philippines. The Europe and North Atlanitic is dominated by a vast high pressure anomaly. At 500 hPa, a significant positive geo-potential high (H) anomaly center is located over central Siberia, which favors development of a blocking high over this region. In the meanwhile, a pronounced positive H center covers northwestern Pacific and extends eastward, associated with an anticyclonic wind center prevailing over the ocean areas south of Japan islands. It favors a northwestward WPSH. Over the Tibetan Plateau a huge low pressure system prevails, associated with the Tibetan Plateau warming (Bao et al. 2010).

To objectively quantify the variability of the third principal mode and to facilitate understanding the influences of local and remote forcing on the mode, it is helpful to pinpoint the most sensitive circulation variability centers with the third principal mode. Boxes in Fig. 3 show the key regions in the SLP, low-level winds and 500 hPa H that are best correlated with the PC3. The third principal mode may be gauged by the SLP anomaly difference between northern EA (25°–50°N, 105°–150°E) and Tibetan Plateau (25°–37°N, 75°–93°E) with a correlation coefficient 0.68

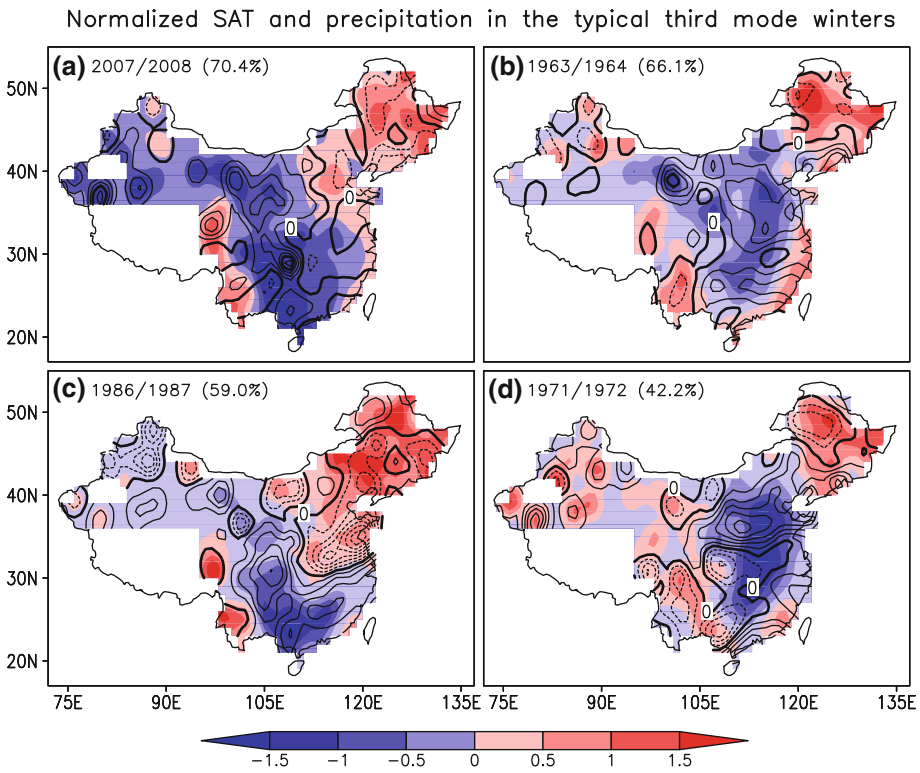

Fig. 2 Observed precipitation (*contours*) and SAT (*shadings*) anomalies over China in **a** 2007/2008, **b** 1963/1964, **c** 1986/1987, and **b** 1971/1972 winters. For convenience of comparison, the sign of Fig. 2c is reversed. The *numbers* in the *brackets* indicate fractional variance of SAT explained by the third EOF mode in Fig. 1. Note precipitation and SAT anomalies have been normalized by climatological means and standard deviations for the period 1957–2008, thus they are non-dimensional

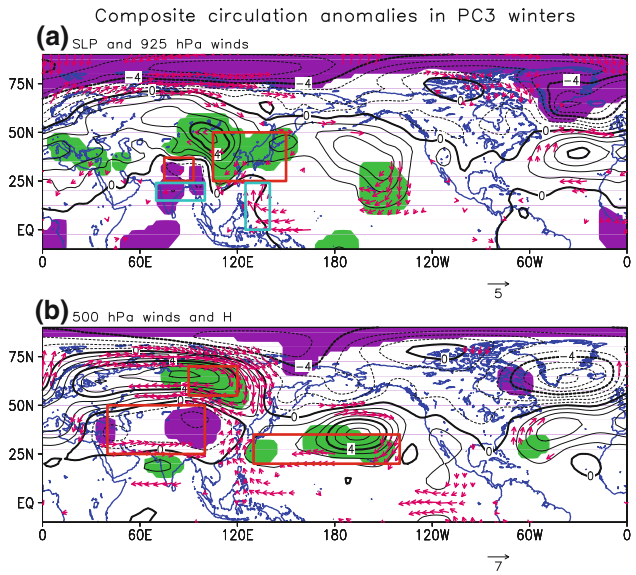

Fig. 3 *Upper panel* **a** Composite difference of DJF sea level pressure (SLP) (*contours* hPa) and 925 hPa winds (*vectors* m/s) between high and low PC3 winters (high minus low). *Lower panel* **b** same as in **a** but for 500 hPa winds (*vectors* m/s) and geopotential height (H) (*contours* 10 gpm). The *green* (*purple*) *shadings* denote *positive* (*negative*) H anomalies exceeding 95% confidence level. The plotted winds are beyond 95% confidence level. The *color boxes* denote geographic regions that define the indicators for the third mode winter

(Fig. 3a). This indicates that a strengthening continental High over northern EA and a weakening Tibetan High are two major circulation features accompanies by a strong third principal mode. The third principal mode can also be measured by the averaged meridional winds over (0°–25°N, 125°–140°E) and zonal winds over (15°–25°N, 70°–100°E) with a correlation coefficient 0.55 (Fig. 3a). It implies that a high third mode winter is usually associated with enhanced moisture transport from the western Pacific, South China Sea and Bay of Bengal. In terms of 500 hPa H, the third principal mode can be best quantified by the H difference between central Siberia (55°–70°N, 90°–120°E), central North Pacific (20°–35°N, 130°–140°W) and TP (25°–50°N, 40°–100°E) (namely, H(Siberia) + H(North Pacific) − H(TP)), with a correlation coefficient 0.71 (Fig. 3b). This means that a strong third principal mode is characterized by enhanced blocking high over central Siberia, intensified WPSH with a northwestward shift and weakened TP high. Based on the results in Fig. 3, we propose that the variability of third principal mode of the EAWM can be measured by the above circulation indices.

4 Origins and predictability sources of the third principal mode

In order to reveal origins and possible sources of predictability of the third principal mode, we investigate the preceding autumn SST anomalies (SSTAs) and sea ice concentration anomalies (SICAs) associated with this mode.

Figure 4 shows the correlation between PC3 and autumn SIC (SST). There are some major significant correlation areas in autumn relevant to the third principal mode. One is the anomalously negative SIC correlation area located in Arctic Ocean (120°E–160°W) (Fig. 4a). Another is the anomalously positive SST correlation area covering the Arctic Ocean areas adjacent to the northern Eurasian continent. The positive SST correlation is quite likely relevant to the negative SICA correlation, because SST warming always favors SIC decreasing. In spite of the SICAs lack of persistence, the SSTAs can persist through the winter (not shown). This might explain the simultaneous 500 hPa H positive correlations over the northern Eurasian continent as shown in Fig. 3b, since the local low boundary heating (cooling) during the high (low) PC3 winters can induce the positive (negative) H anomalies over this region.

It is interesting to notice that no significant correlation is found with tropical SST in the prior autumn, while large areas of significant correlations are detected with extra-tropical SST in North Pacific (Fig. 4b) and sustain through the winter (not shown). This indicates that the third mode is more likely to result from the extra-tropical SSTA than ENSO. This result is different from the argument in the previous studies that ENSO provided a condusive condition for the snowstorms in 2007/2008 winter.

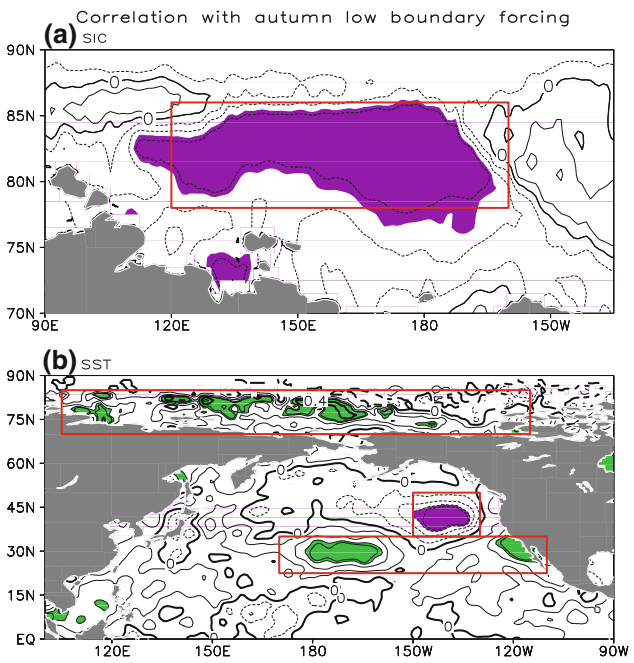

Fig. 4 Correlation between PC3 and autumn **a** sea ice concentration (SIC), **b** sea surface temperature (SST). The contour interval is 0.1. The *green* (*purple*) *shadings* denote *positive* (*negative*) correlation coefficients exceeding 95% confidence level. The *red boxes* denote geographic regions that define the predictors for the third mode winter

Those features derived from the above correlation analysis can also be observed in the composite analysis between the high and low PC3 winters (not shown). The SSTAs bear a similar pattern with that in Fig. 4b from prior autumn to winter. Such SSTA persistence provides predictability sources for the third principal mode winters. The Arctic SICAs varies significantly from prior autumn to winter in the composite analysis, which is most likely due to the flowability of the sea ice. Such flowability limits its capacity as a predictability source of the abnormal EAWM. However, the effects of the Arctic SICAs may be reflected by SSTAs in the Arctic Ocean areas adjacent to the northern Eurasian continent.

To summarize, it may be speculated that the SSTAs in the Arctic Ocean areas adjacent to the northern Eurasian continent and those in extra-tropical North Pacific are two major origins and predictability sources of the third principal mode of the EAWM.

5 Physical mechanisms

In this section, we discuss the physical processes through which the lower boundary forcing affects the EAWM variability with the SGCM. To mimic the diabatic heating effects of the SSTAs in Arctic, central North Pacific and northeastern Pacific, we imposed two heating sources and one cooling source; each has an elliptical squared cosine distribution in latitude and longitude with a vertically integrated heating rate of 2.5 K/day which is approximately the latent heating rate release given by an extra 10 mm precipitation per day (right panel in Fig. 5). The magnitude of heating anomaly imposed here is according to the previous work by Hoskin and Karoly (1981). To make the numerical results more robust, the control run was integrated for 12 years and the last 10 years' integration was used to derive a reference state. The sensitivity tests were integrated for 10 years each. The 10-year integrations were used to construct a 10-member ensemble (arithmetic) mean to reduce the uncertainties arising from differing initial conditions. To isolate the roles of the Arctic SSTAs and the Pacific SSTAs, first we perform sensitive experiments with the Arctic forcing and the Pacific forcing, separately.

It can be clearly seen from Fig. 6a that under the Arctic SSTA forcing, 550 hPa H basically responds an anomalously positive anomaly center located over northern Eurasian continent, which may favor developing and sustaining of the blocking high over this area. Figure 6b displays that there are two significant 550 hPa H anomaly centers as responses to the Pacific SSTA forcing. This pattern favors the enhancement and northwestward shift of the WPSH. The physical mechanisms are interpreted as

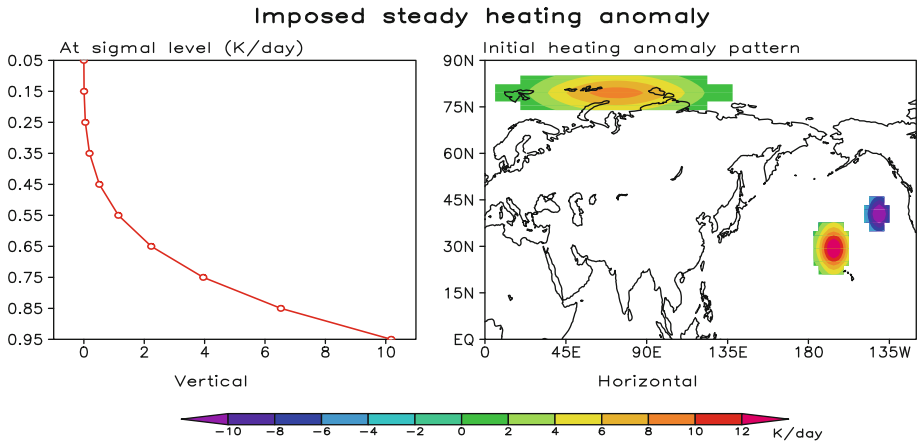

Fig. 5 Specified diabatic heating profiles (*curves* in the *left panel*) and imposed SST anomaly (SSTA) (*color shadings* in the *right panel*) for a high PC3 forcing in the numerical experiment with the simplified general circulation model (SGCM). Maps for a low PC3 forcing are mirror images of the plot shown here

follows. The warming (cooling) SSTA usually favors high (low) H anomalies due to the sensible heating as the experiments show. On the other hand, high (low) H anomalies would enhance (weaken) solar radiation and maintain the warming (cooling) SSTA. Such positive feedback may sustain such air-sea anomaly pattern.

Figure 7 shows responses of the atmosphere to forcings from both the Arctic and Pacific. The 550 hPa H simulation basically captures the major features of the third principal mode of the EAWM, namely, enhanced blocking high over central Siberia and intensified WPSH with a northwestward shift. It further verified the speculation in Sect. 5 that the Arctic SSTAs and the SSTAs in the extra-tropical Pacific are two major origins and predictability sources of the third principal mode of the EAWM (Fig. 8).

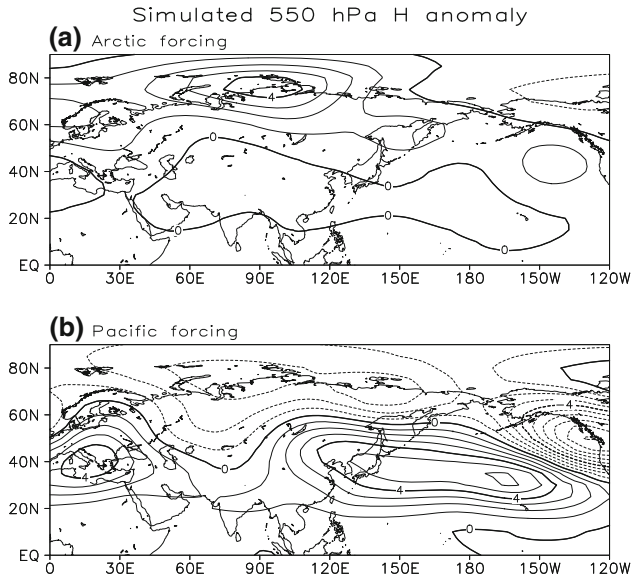

Fig. 6 550 hPa H (*contours* in units of m) responses to the **a** Arctic forcing and **b** Pacific forcing in the SGCM, respectively

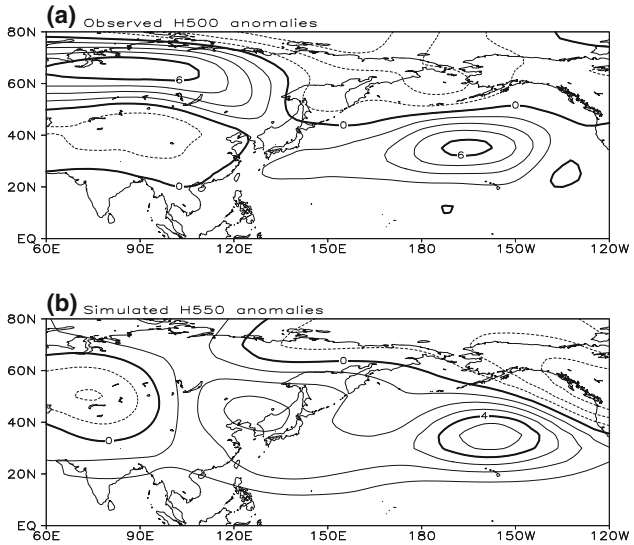

Fig. 7 **a** Observed H500 difference between the high and low PC3 winters and **b** simulated 550-hPa H responded to both Artic and Pacific forcing in the SGCM (*contours* in units of 10 gpm)

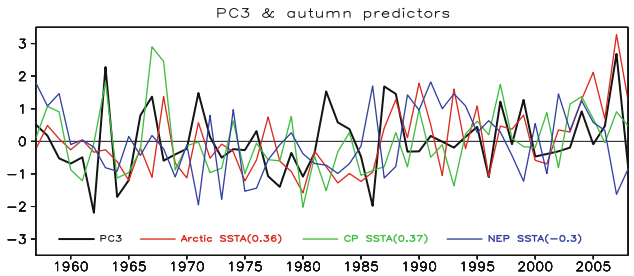

Fig. 8 Time series of PC3 (*black curve*) and the SSTA in Arctic (*red curve*), central North Pacific (CP) (*green curve*) and northeastern Pacific (*blue curve*) in the preceding autumns from 1957 through 2008. The correlation coefficients are indicated in the *brackets*

6 Seasonal prediction

To study how well the above predictability sources contribute to the prediction skill of the EAWM third mode

(Fig. 8), an empirical seasonal prediction model is developed using a linear regression method for the period of 1957–2008 (see Eq. 1).

$$y = 0.3 \cdot x_1 + 0.26 \cdot x_2 - 0.32 \cdot x_3 \quad (1)$$

where x_1, x_2 and x_3 denotes the prior autumn SSTAs averaged in the Arctic Ocean (70°–85°N, 105°E–115°W), central North Pacific (22.5°–35°N, 170°E–110°W) and northeastern Pacific (35°–50°N, 150°–130°W), respectively (Fig. 8). The correlation between the simulation and the observation of the PC3 is 0.55.

To test the predictive capability of the empirical model, the cross validation method is performed to hindcast the PC3 (1957–2008) (Michaelsen 1987; Wu et al. 2009b). To warrant the hindcast result robust, we choose a leaving-thirteen-out strategy (Blockeel and Struyf 2002). The relevant procedures are as following: The cross-validation method systematically deletes 13 years from the period 1957–2008, derives a forecast model from the remaining years, and tests it on the deleted cases. Note that the choice of "leaving-thirteen-out" is not random. Blockeel and Struyf (2002) suggested that randomly choosing 20–30% of the data to be in a test data and the remainder as a training set for performing regression can prevent overfitting or wasting data. In our paper, 25% of the whole hindcast period (52 years) equals to 13 years. That's why we choose a leaving-thirteen-out strategy. The cross-validated estimates of the PC3 are shown in Fig. 9. The correlation coefficient between the observation (black line in Fig. 9) and the 52-year cross-validated estimates of the empirical model (red line in Fig. 9) is 0.45. To verify the prediction skill in real forecast, we apply a 30-year moving training window prior to forecast year and perform a 10-year real forecast from 1999/2000 winter through 2008/2009 winter (Fig. 10). The correlation coefficient between the observation and the real forecast is 0.59, exceeding 95% confidence level. The 2007/2008 abnormal EAWM is realistically forecast, even better than the hindcast. It indicates that this empirical seasonal prediction model does show a promising skill in predicting the extreme phase of the abnormal EAWM as 2007/2008 winter. Since all these predictors can be readily monitored in real time, this empirical model provides a real time forecast tool and may facilitate the seasonal prediction of high-impact weather associated with the abnormal EAWM.

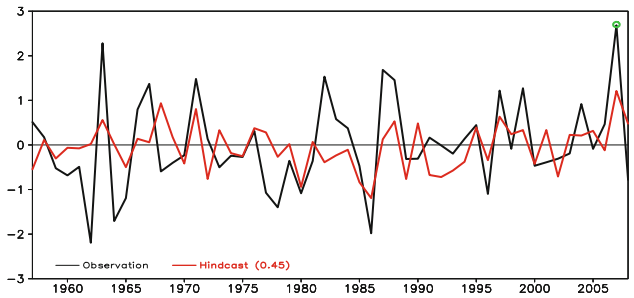

Fig. 9 Time series of the observed PC3 (*black curve*), its cross-validated hindcast made by the empirical model (*red curve*) and the 22-year real forecast for the 1987–2008 period with 30-year moving training window prior to forecast year (*green curve*). The correlation coefficient is indicated in the brackets. The *green blank circle* denotes 2007/2008 winter

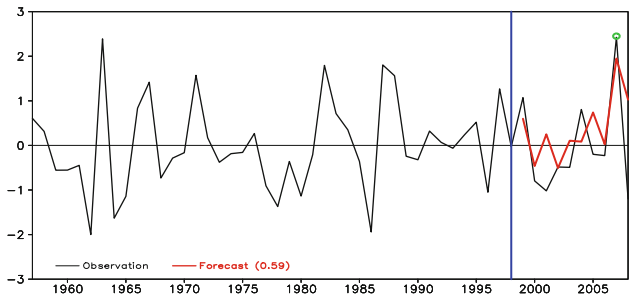

Fig. 10 Time series of the observed PC3 (*black curve*) and the 10-year real forecast for the 1999–2008 period with 30-year moving training window prior to forecast year (*green curve*). The correlation coefficient is indicated in the *brackets*. The *green blank circle* denotes 2007/2008 winter. The *blue vertical line* refers to 1998/1999 winter prior to the real forecast starts

7 Conclusion and discussion

Using observed data over the past 52 years (1957–2008), this study attempts to unveil the origins and predictablility sources of the third principal mode of the EAWM which dominated 2007/2008 winter over EA. Although the third principal mode explains only 8.7% of the total SAT variance over EA, it can bring about huge catastrophic consequences such as the 2007/2008 once-in-a-century snowstorms over EA. This mode is significantly different from the first two leading modes documented by Wang et al. (2010). It is characterized of an increased surface pressure over the northwestern EA, an enhanced CSH, and a strengthened and northwestward extended WPSH. Preceded the anomalous third mode EAWM winters, large areas of SSTAs are observed in prior autumn in the Arctic Ocean areas adjacent to northern Eurasian continent, central North Pacific and northeastern Pacific as well as with the prominent Arctic sea ice concentration anomalies. The SSTAs can persist through ensuing winter, which offers predictability sources for the third mode. The flowability of the SICAs decreases their predictability. However, the Arctic SICAs on the origin of the third EAWM mode may be very critical based on the above results. Their effects can be reflected by changing the Arctic SSTAs.

To further understand the physical process responsible for circulation anomalies associated with the third principal mode, three numerical experiments are designed

with the SGCM to see atmosphere responses to the forcings originated from the Arctic and the extra-tropical Pacific. Results demonstrate that the Arctic SSTAs excite geo-potential height anomalies over northern Eurasian continent and impacts on the CSH, while the extra-tropical North Pacific SSTAs deforms the WPSH and Aleutian Low. Co-effects of them play crucial roles on origins of the third EAWM mode and may provide predictability sources of the extreme phases of this mode. Based on these results, an empirical model is established to predict the third mode of the EAWM. Hindcast is performed for the 1957–2008 period, which shows a quite realistic prediction skill in general and good prediction ability in the extreme phase of the third mode of the EAWM such as 2007/2008 winter. Since all these predictors can be readily monitored in real time, this empirical model provides a real time forecast tool and may facilitate the seasonal prediction of high-impact weather associated with the abnormal EAWM.

However, the SGCM simulation in Fig. 7b has biases compared with the observation, especially over the Eurasian continent (Fig. 7a). The discrepancy may come from the model itself and the existence of other predictability sources. The third mode of the EAWM may have other predictability sources, because our empirical model hindcast explains around 20% of the observational variance (their correlation coefficient being 0.45). Due to data limitation, we only find three predictors. If more and better data are available, the feasibility of finding other predictability sources will increase, correspondingly. Besides the above physical approaches, application of a better mathematic strategy of model construction may also improve seasonal prediction skill (e.g., Li and Smith 2009). This is based on the fact that although many physical processes are not fully understood up to now, they can be well depicted, mathematically. How to perfectly combine these two approaches is still an open issue. This work is just a beginning and much more future work needs to do be done to improve seasonal prediction skill of these high impact climate events.

Acknowledgments Zhiwei Wu is supported by the Sustainable Agriculture Environment Systems (SAGES) research initiative of Agriculture and Afri-Food Canada through the Natural Sciences and Engineering Research Council of Canada (NSERC) Fellowship Program. The authors are supported by the Special Research Program for Public Welfare (Meteorology) of China under Grant No. GYHY200906016 and the National Basic Research Program "973" (Grant No. 2010CB950400).

References

Bao Q, Yang J, Liu YM, Wu GX, Wang B (2010) Roles of anomalous Tibetan Plateau warming on the severe 2008 winter storm in central-southern China. Mon Wea Rev. doi:10.1175/2009MWR2950.1

Blockeel H, Struyf J (2002) Efficient algorithms for decision tree cross-validation. J Mach Learn Res 3:621–650

Chan J, Li C (2004) The East Asia winter monsoon. In: Chang C-P (ed) East Asian Monsoon. World Scientific, Singapore, pp 54–106

Chang CP, Wang Z, Hendon H (2006) The Asian winter monsoon. In: Wang B (ed) The Asian monsoon. Praxis, New York, p 89

Chang CP, Lu MM, Wang B (2009) The East Asian winter monsoon. In: Chang C-P et al (eds) The global monsoon system: research and forecast, 2nd edn. World Scientific, Singapore (in press)

Ding YH, Krishnamurti TN (1987) Heat budget of the Siberian high and the winter monsoon. Mon Wea Rev 115:2428–2449

Ding YH, Wang ZY, Song YF, Zhang J (2008) Causes of the unprecedented freezing disaster in January 2008 and its possible association with the global warming. Acta Meteorologica Sinica 665:809–825

Hall NMJ (2000) A simple GCM based on dry dynamics and constant forcing. J Atmos Sci 57:1557–1572

Hong CC, Li T (2009) The extreme cold anomaly over southeast Asia in February 2008: roles of ISO and ENSO. J Clim 22:3786–3801

Hoskin BJ, Karoly DJ (1981) The steady linear response of a spherical atmosphere to thermal and orographic forcing. J Atmos Sci 38:1179–1196

Hoskins BJ, Simmons AJ (1975) A multi-layer spectral model and the semi-implicit method. Quart J Roy Meteor Soc 101:637–655

Jhun JG, Lee EJ (2004) A new East Asian winter monsoon index and associated characteristics of winter monsoon. J Clim 17:711–726

Li XZ (1955) A study of cold waves in East Asia. Offprints of scientific works in modern China–meteorology (1919–1949) (in Chinese). In: Li XZ (eds). Science Press, Beijing. pp 35–117

Li S, Bates G (2007) Influence of the Atlantic Multidecadal Oscillation on the winter climate of East China. Adv Atmos Sci 24(1):126–135

Li Y, Smith I (2009) A statistical downscaling model for southern Australia winter rainfall. J Clim 22:1142–1158

Lin H, Derome J (1996) Changes in predictability associated with the PNA pattern. Tellus 48A:553–571

Michaelsen J (1987) Cross-validation in statistical climate forecast model. J Clim Appl Meteor 26:1589–1600

North GR, Bell TL, Cahalan RF et al (1982) Sampling errors in the estimation of empirical orthogonal functions. Mon Wea Rev 110:699–706

Rayner NA, Parker DE, Horton EB, Folland CK, Alexander LV, Rowell DP, Kent EC, Kaplan A (2003) Global analyses of sea surface temperature, sea ice, and night marine air temperature since the late nineteenth century. J Geophys Res 108:D14407. doi:10.1029/2002JD002670

Tao SY (1957) A study of activities of cold airs in East Asian winter, Handbook of Short-Term Forecast (in Chinese), China Meteorological Administration (eds). Meteorology Press, Beijing, pp 60–92

Tao SY, Wei J (2008) Severe snow and freezing rain in January 2008 in the southern China. Climatic Enviro Res (in Chinese) 13(4):337–350

Uppala S, Kallberg PW, Simmons AJ et al (2005) The ERA-40 reanalysis. Quart J Roy Meteor Soc 131:2961–3012. doi:10.1256/qj.04.176

Wang DH, Liu CJ, Liu Y, Wei FY, Zhao N, Jiang ZN, Li Y, Chen JY, Wang YF, Shi XH, Xu XD (2008) A preliminary analysis of features, causes of the snow storm event over the Southern China in January 2008. Acta Meteorologica Sinica 66(3):405–422

Wang B, Wu ZW, Chang CP, Liu J, Li JP, Zhou TJ (2010) Another look at interannual to interdecadal varaitions of the East Asian winter monsoon. J Clim (in press)

Wen M, Yang S, Kumar A, Zhang P (2009) An analysis of the large-scale climate anomalies associated with the snowstorms affecting China in January 2008. Mon Wea Rev 137:1111–1131

Wu ZW, Li JP, Wang B, Liu XH (2009a) Can the Southern Hemisphere annular mode affect Chinese winter monsoon? J Geophys Res 114:D11107. doi:10.1029/2008JD011501

Wu ZW, Wang B, Li JP, Jin FF (2009b) An empirical seasonal prediction model of the East Asian summer monsoon using ENSO and NAO. J Geophys Res 114:D18120. doi:10.1029/2009JD011733

Zheng GG (2008) An extremely rare snowstorm and freezing disaster. Meteorol Knowl (in Chinese) 28(1):4–6